e-Journal of Nondestructive Testing - ISSN 1435-4934 - www.ndt.net

EWSHM 2024
11th European Workshop on Structural Health Monitoring

Analyzing Vertical Earthquake Vibrations and Moving Vehicle Loads for Structural Health Monitoring and Vibration Suppression in Bridges

Ardalan BAHRAMI ESKANDARI [1], Ali NIKKHOO [2], Iman HAJIRASOULIHA [3]
[1]Bundesanstalt für Materialforschung und -prüfung (BAM), division 8.2, Berlin, Germany, ardalan.bahrami-eskandari@bam.de
[2] The University of Science and Culture, Department of Civil Engineering, Tehran, Iran, nikkhoo@usc.ac.ir
[3] The University of Sheffield, Department of Civil and Structural Engineering, Sheffield, United Kingdom, i.hajirasouliha@sheffield.sc.uk

Abstract. The design of bridges often overlooks the vertical component of earthquakes or considers it of secondary importance, despite compelling evidence indicating specific structural damage caused by primary earthquake waves. Conversely, during the operational phase, the combined influence of ground motion and moving loads from vehicles can significantly impact the structural health monitoring (SHM) of bridges. This study aims to evaluate the simultaneous effect of vertical earthquake vibrations and moving vehicle loads on simply supported bridges. The research employs a practical methodology based on the eigenfunction expansion method to analyze change of deflection due to the effect of these concurrent forces under seven different earthquake records. It is shown that within a realistic range of vehicle mass and velocity, the average of changing the maximum deflection at the mid-span of the main beam (denoted as M_n) reaches up to 163% under various scenarios. Subsequently, the seismic parameters influencing this phenomenon are identified through a statistical analysis of set of 100 different earthquake records with unique features. A linear regression equation is presented to predict the M_n based on the earthquake specific properties. Additionally, to control the vertical vibration of bridge systems, a novel vibration suppression system utilizing steel pipe dampers is introduced, and its reliability is examined across a broad spectrum of bridge flexural rigidity. The results indicate that the system's efficiency depends on M_n and the soil type of the bridge construction, enabling a reduction in structural sections (up to 27%) while achieving the same maximum target deflection in the initial state. This efficiency leads to a more economical design solution, emphasizing the potential benefits of the proposed system for practical application.

Keywords: Bridge structures, Vertical earthquakes, Moving vehicles, Suppressing vibrations, Health monitoring

https://doi.org/10.58286/29746

Introduction

Modelling bridge structures using various beam theories such as Euler-Bernoulli Beam Theory (EBT), Timoshenko Beam Theory (TBT), Higher Order Beam Theory (HOBT), or Finite Element Method (FEM) is integral to the analysis of bridge structures [1,2,3,4]. These theories account for external loading in both ultimate and operational phases, providing critical insights into the behaviour of bridges under different conditions. However, recent studies have highlighted the significance of considering the vertical component of earthquakes, which has often been overlooked or given secondary attention in design processes [5,6]. Reliability analysis plays a crucial role in ensuring the structural integrity of bridges. Methods such as First and Second Order of Reliability Methods (FORM and SORM) have been instrumental in assessing the reliability of bridge designs [4,7]. Additionally, investigations into bridge base excitation, structural frequency content, shape functions, and deflections have been prominent in the past two decades, contributing to a deeper understanding of bridge behaviour [2,4,5,8].

This study focuses on employing Euler-Bernoulli Beam Theory (EBT) and shape functions to model continuous parameter structures under external dynamic loading from moving vehicles and vertical ground motion during the operational phase of bridge structures. Furthermore, the Eigenfunctions Expansion Method (EEM) is utilized to determine the maximum deflection of the bridge main beams. Comparing maximum deflections between two scenarios, collective loading of earthquakes and moving masses versus single loading without earthquakes, highlights the simultaneous effect denoted as M_n. Statistical analysis, encompassing various scenarios, has yielded a regression mathematical relationship to predict and underscore the importance of considering vertical components in bridge design processes. Moreover, this study proposes the implementation of a novel passive steel pipe damper (SPD) for the main beams to suppress vibrations. It is demonstrated that section dimensions can be reduced through SPDs usage, with their efficiency directly correlated to construction soil type (V_s30 (m/s)) and the M_n factor.

1. Numerical Modelling

1.1 Main Beam of Bridge Structure

Considering a uniform undamped Euler-Bernoulli simply supported beam with the length of $L = 60\ m$, mass per unit length of $\rho A = 2956\ kg/m$ and flexural rigidity of $EI = 3.467 * 10^{10}\ N\ m^2$ [6] leads the equation 1 as follows [8]:

$$\rho A\ \frac{\partial^2 D(x,t)}{\partial t^2} + EI\ \frac{\partial^4 D(x,t)}{\partial x^4} = f(x,t) \quad (1)$$

Where $D(x,t)$ indicates the vertical displacement function along the beam length at time t domain.

1.2 External Dynamic Loading

The function $f(x,t)$ in equation (1) represents the external dynamic loading, which is considered in two different states: i) The effect of 15 traveling vehicles with $m = 5000\ kg$ and $v = 30\ m/s^2$ which cross at uniform intervals of $d = L/2$ [5] is denoted as $f(x,t)_i$. Equation (2) details the single loading considering this fact that the vehicles are not separated from the beam during vibration.

$$f(x,t)_i = \sum_{k=1}^{15} m\,[\,g - \left\{\frac{\partial^2 D(x,t)}{\partial t^2} + 2v\frac{\partial^2 D(x,t)}{\partial x \partial t} + v^2\frac{\partial^2 D(x,t)}{\partial x^2}\right\}_{x=v(t-t_k)}]\,.\,(\delta\,[\,x - v(t-t_k)].\Delta H(t)) \quad (2)$$

Where t_k is the time of arrival of the kth vehicle and δ denotes the Dirac delta function. The action of kth mass is considered by the unit step function $\Delta H(t) = H(t-t_k) - H\left(t - t_k - \frac{L}{v}\right)$, when the load enters and departs from the beam, correspondingly. ii) The second scenario occurs by applying the vertical ground motion to the bridge structure while the moving masses cross simultaneously over the bridge length during the operation phase. The bridge response in this scenario termed as simultaneous effect.

$$f(x,t)_{ii} = f(x,t)_i - \{\rho A + \sum_{k=1}^{N} m\,.\,\delta\,[\,x - v(t-t_k)].\Delta H(t)\}.\ddot{U}_g(t) \quad (3)$$

Where $\ddot{U}_g(t)$ is the earthquake acceleration at time t. To investigate the effect of different frequency content of earthquakes, the vertical component of seven different near-field earthquakes based on table 1 is chosen.

Table 1. Earthquake specifications [5].

Number	1	2	3	4	5	6	7
Event	L'Aquila, Italy	Imperial Valley-02	Kobe, Japan	Mammoth Lakes-01	Loma Prieta	Northridge-01	Tabas, Iran
Year	2009	1940	1995	1980	1989	1994	1978
Station	GRAN SASSO (Assergi)	El Centro Array #9	KJMA	Convict Creek	Corralitos	Arleta - Nordhoff Fire Sta	Tabas
Magnitude	6.3	6.95	6.9	6.06	6.93	6.69	7.35
Soil type	C	D	D	C	C	D	B
Rjb (km)	6.35	6.09	0.94	1.1	0.16	3.3	1.79
Vs30 (m/s)	488	213	312	382	462	298	767
PGA (H)	0.150g	0.281g	0.834 g	0.442g	0.645g	0.345g	0.862g
PGA (V)	0.110g	0.178g	0.339g	0.387g	0.458g	0.552g	0.641g

1.3 Problem Solving

Employing the Characteristic Orthogonal Polynomials (COPs) [1] as well as using the direct method for simply supported beams [5], resulted in the computation of the orthogonal shape function for the ith beam vibration mode ($\varphi_i(x)$)). On the other hand, the eigenfunction expansion method (EEM) in the form of $D(x,t) = \sum_{i=1}^{p} \varphi_i(x) a_i(t)$, is used to solve the differential equation. Where p is the total required number of shape functions and $a_i(t)$ is the corresponding amplitude for the ith time-dependent amplitude. The final matrix equation (4) is extracted by applying the EEM to the equation (1) along with equation (2) or (3), depending on single or the collective scenario, and multiplying both sides by $\varphi_j(x)$, integrating over the beam length (L), and applying the orthogonal perpendicular principle. Numerical methods can be employed to solve the matrix equation in the t domain [3,5].

$$\boldsymbol{M(t)}\frac{d^2\boldsymbol{a(t)}}{dt^2} + \boldsymbol{C(t)}\frac{d\boldsymbol{a(t)}}{dt} + \boldsymbol{K(t)a(t)} = \boldsymbol{F(t)} \quad (4)$$

2. Simultaneous Effect

2.1 Changing the Maximum Deflection (M_n)

To study the simultaneous effect, we compute the maximum deflection at mid-span in single and collective type of loading and investigate the variations by the M_n factor.

$$M_n = \frac{D(\frac{L}{2},t)_{ii} - D(\frac{L}{2},t)_i}{D(\frac{L}{2},t)_i} * 100 \quad (5)$$

The results in Table 2 imply a 43.4% increase in the average of simultaneous effects under the seven different earthquakes. The M_n in Kobe and Tabas are more prominent, showcasing up to twice the values.

Table 2. Impact of vertical earthquake excitation on maximum deflections at beam's mid-span [5].

Number	Earthquake Event	Maximum mid-span beam deflection (m)		Impact of vertical earthquake excitation on mid-span deflection M_n (%)
		Moving mass	Moving mass + Earthquake	
1	L'Aquila, Italy	0.133	0.138	3.8
2	Imperial Valley-02	0.133	0.141	6.0
3	Kobe, Japan	0.133	0.270	103
4	Mammoth Lakes-01	0.133	0.177	33.1
5	Loma Prieta	0.133	0.165	24.1
6	Northridge-01	0.133	0.180	35.3
7	Tabas, Iran	0.133	0.264	98.5

Figure 1 shows the mid-span beam deflection time-history response of the case study bridge due to moving masses (dash line) and the simultaneous effects (solid line). The seismic loads amplify the effects of moving vehicles in most cases, resulting in deflections up to twice.

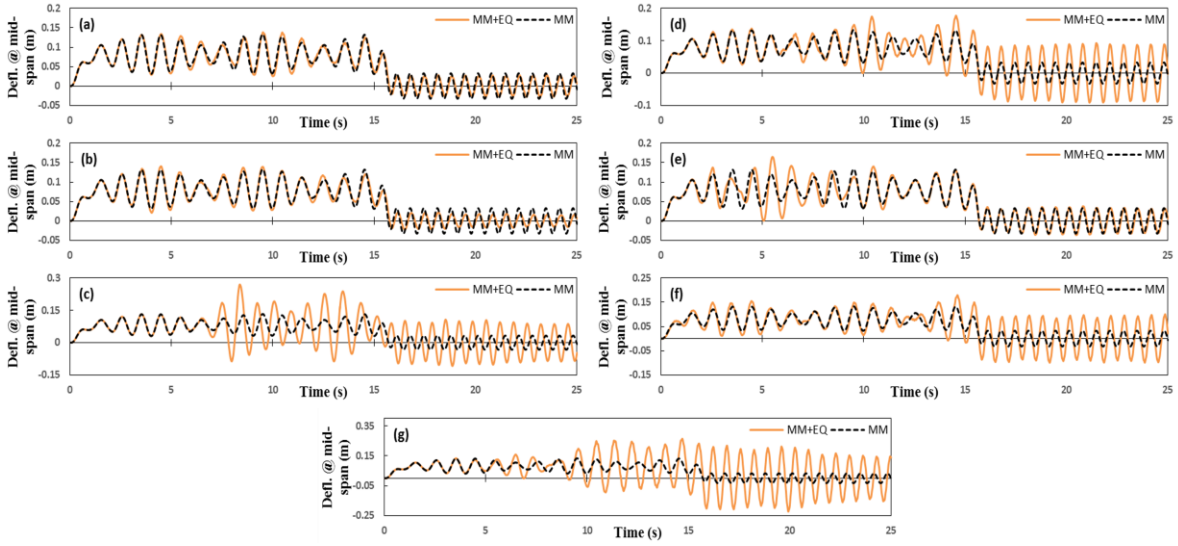

Fig. 1. Time-history Deflection of the Beam due to External Excitations. a) L'Aquila, b) Imperial Valley, c) Kobe, d) Mammoth Lakes, e) Loma Prieta, f) Northridge, g) Tabas [5].

2.2 Parametric Study of Moving Masses

To investigate the effect of moving masses variation on the bridge responses under the simultaneous effect, we study velocity(v), mass(m) and determined distance(d) of moving masses through non-dimensionalization by the factors of $M_{normalized} = \rho A * L$ and $V_{normalized} = \frac{2*L}{T_1}$, where T_1 is the period of the first mode of the main beam [1]. Hence, based on the bridge specifications [6], $M_{normalized}$ and $V_{normalized}$ are equal to 177360 kg and 179 m/s^2, respectively. The determined distance between two moving vehicles is calculated at 6 meters per speed per 15 km/h, following typical driving regulations. Therefore, the distance between moving masses can be calculated as $d = 1.44 * v$. The common non-dimensional interval on actual examples for $M/M_{normalized}$ and $v/v_{normalized}$ is between 0.05 and 0.35 [1,8]. Table 2 shows the average and maximum results of M_n in this interval under different earthquake scenarios. The average results increase up to 163% in the Tabas, while they show noticeable values also under the other earthquakes. These findings imply the importance of consideration vertical components of earthquakes in the bridge design process under different types of moving masses loading.

Table 3. Impact of vertical earthquake excitation on maximum deflections at beam's mid-span.

Number	Earthquake events	Average of M_n (%)	Maximum of M_n (%)
1	L'Aquila, Italy	13.04	104.59
2	Imperial Valley-02	11.13	80.87
3	Kobe, Japan	147.62	747.69
4	Mammoth Lakes-01	71.54	401.24
5	Loma Prieta	80.55	342.80
6	Northridge-01	28.49	219.50
7	Tabas, Iran	163	513.80

2.3 Parametric Study of Earthquake

Based on previous findings, the response of M_n is significantly influenced by the phenomena of earthquakes and their frequency content. To investigate the effect of different earthquakes on the M_n response, a statistical study on the bridge response under applying 100 different near/far-field (R_{jb}<10 or R_{jb}>10) earthquakes is conducted. Moving masses are assumed with the initial modelling ($m = 5000\ kg$, $v = 30\ m/s^2$ and $d = L/2$). Table 4 shows the range of different parameters for 100 selected earthquakes.

Table 4. Range of 100 selected earthquake parameters.

Number	Parameter	Minimum	Maximum
1	Magnitude (M_w)	5	7.9
3	Soil type (V_s30)	< 175	> 750
4	(PGA_H)	0.009 g	1.494 g
5	(PGA_V)	0.004 g	2.281 g
6	(PGA_H/PGA_v)	0.509	5.645

Figure 2 displays the histogram of M_n responses for 100 selected earthquakes on the main bridge beam origin. These responses, with a minimal disparity between the standard deviation (STDEV) of 23.6 and the average (AVG) of 18.1, are suitable for statistical analysis. The bar chart shows an asymmetric right-skewed normal distribution, concentrated within the 0 to 40% range. The findings indicate that simultaneous effects are prevalent, with

the majority exhibiting a positive M_n response. The Linear Least Squares Method (LLSM) predicts simultaneous effect response statistically, with PGA_V and Earthquake Magnitude (M_w) being the most influential contributors based on their "P-value" and "Standardized Coefficients Beta." Equation 6 presents a linear regression model for extracting structural response, exhibiting a significant correlation (Multiple R = 0.652). while the model explains 42% of the variances in the M_n response (Adjusted R Square), indicating a substantial mathematical relationship for the responses under the earthquake phenomena.

$$M_n = -27.353 + 5.566\, Mag + 43.685\, PGA_V \tag{6}$$

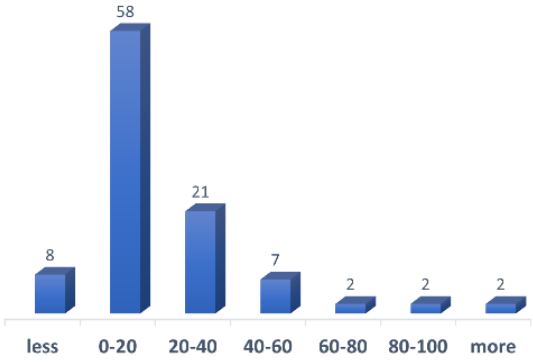

Fig. 2. Histogram of M_n bridges response under 100 selected earthquakes

3. Vibration Suppression

3.1 Steel Pipe Dampers (SPDs)

Steel pipe dampers have been shown to be effective in engineering design due to their ability to exhibit stable hysteresis behaviour and absorb significant energy through metallic yielding [9]. Therefore, they have been chosen for this study to mitigate the impact of simultaneous effect. Figure 3 shows the conceptual representation of steel pipe dampers integrated along the primary bridge beam.

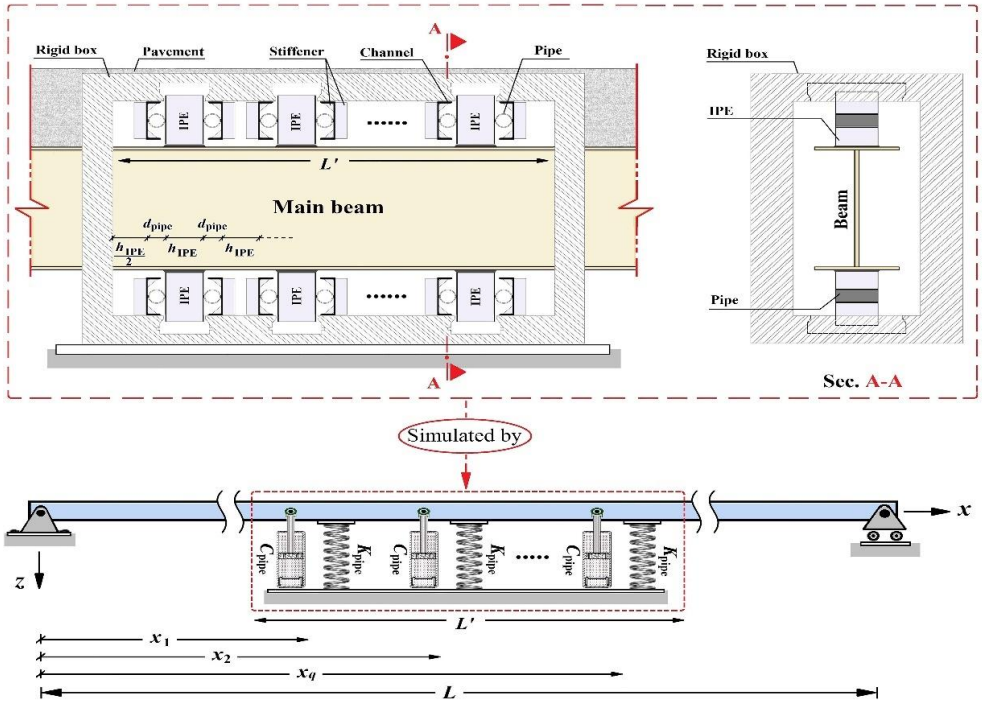

Fig. 3. Schematic view of the steel pipe dampers along the main beam [5].

The box comprises multiple pipes with an external diameter of d_{pipe} attached to the mid-span of the main bridge beam, where the maximum deflection occurs. It is assumed that the rigid box responds independently of the main beam, thus not affecting the beam's deformation under external forces. The damping factor of each pipe damper (C_{pipe}) is calculated using $C_{pipe} = 2\mu(M_{pipe} \cdot K_{pipe})^{0.5}$, where M_{pipe} is the mass of each pipe in kilograms. The external diameter of the pipe dampers, d_{pipe}, is set to $119\,mm$, with a damping ratio (μ) of 0.4 [9]. The stiffness factor of the pipe, K_{pipe}, in elastic and plastic deformation zones is given as $0.0034\ l\ kN/mm$ and $0.00017\ l\ kN/mm$, respectively, where l is the length of each pipe in millimetres (mm) [9]. The estimated yield strength (F_y) of the pipe dampers is $0.0088l\ kN$, resulting in a deformation of 2.6 mm [5]. To connect the pipes to the main beam, an IPE270 section is used, and the length of the pipe box L' is chosen to be equal to the sitting length of the beam, which is 3 m for a beam length of 60 m. Therefore, for this case study, the maximum number of pipe dampers is set to 16, which should be a multiple of four as shown in Figure 3. The SPD system (rigid box) response is simulated using a spring-dashpot model. During loading phases, the pipe dampers may enter the plastic phase, while the beam remains in the elastic regime under design load conditions. The stiffness and damping properties of the steel pipes directly affect the vibration of the beam. Therefore, the matrix equation (4) is written as follows:

$$
\begin{aligned}
&\boldsymbol{a(t)} = [\boldsymbol{a_i(t)}]_{\boldsymbol{p\times 1}},\\
&\boldsymbol{M(t)} = \left[\rho A\delta_{ij} + \sum_{k=1}^{15} m\phi_i[v(t-t_k)].\,\phi_j[v(t-t_k)].\,\Delta H(t)\right]_{p\times p},\\
&\boldsymbol{C(t)} = \left[C_{pipe}^{e}\int_{x_1}^{x_q}\phi_i(x)\phi_j(x)dx.\,\Delta H(x) + \sum_{k=1}^{15} 2mv\phi_{i,x}[v(t-t_k)].\,\phi_j[v(t-t_k)].\,\Delta H(t)\right]_{p\times p},\\
&\boldsymbol{K(t)} = \left[\sum_{i=1}^{p}\left\{\sum_{j=1}^{p}\int_0^L EI.\,\phi_{i,xxxx}\phi_j(x)dx\right\} + K_{pipe}^{e}\int_{x_1}^{x_q}\phi_i(x)\phi_j(x)dx.\,\Delta H(x) + \sum_{k=1}^{15} mv^2\phi_{i,xx}[v(t-t_k)].\,\phi_j[v(t-t_k)].\,\Delta H(t)\right]_{p\times p},\\
&\boldsymbol{F(t)} = \left[\left[g - \frac{d^2U_g(t)}{dt^2}\right]\sum_{k=1}^{15} m\phi_j[v(t-t_k)].\,\Delta H(t) - \rho A\frac{d^2U_g(t)}{dt^2}\int_0^L\phi_j(x)dx\right]_{p\times 1}.
\end{aligned}
\tag{7}
$$

In this setup, the equivalent stiffness (K_{pipe}^{e}) and damping (C_{pipe}^{e}) factors of the steel pipe system are determined by $K_{pipe}^{e} = (n_{pipe}.K_{pipe})/(L' - h_{IPE})$ and $C_{pipe}^{e} = (n_{pipe}.C_{pipe})/(L' - h_{IPE})$, respectively, where n_{pipe} is the total number of SPDs. The stiffness factor of each pipe (K_{pipe}) and accordingly its damping factor (C_{pipe}) varies in proportion to the pipe selected and its elastic and plastic deformation zones. Besides, The effect of pipes is considered by the unit step function of $\Delta H(x) = H(x - x_1) - H(x - x_q)$, where x_1 and x_q are the distance between centre of the first and last pipe-couple from the assumed origin, respectively (see Figure 3).

3.2 Efficiency of Steel Pipe Dampers (SPDs) in Vibration Suppression

In Figure 4, the graphs illustrate how the maximum mid-span deflection of the main bridge beam varies with respect to its initial flexural rigidity factor ($K_n = [0.5, 0.6, \ldots, 1] * EI$) under different seismic scenarios. This comparison is made both for a single-span bridge without dampers ($n_{pipe} = 0$) and for the same bridge equipped with steel pipe dampers ($n_{pipe} = 4, 8, 12, 16$). Interestingly, the maximum deflection of bridge systems with steel pipe dampers remains largely unaffected by the initial flexural rigidity factor of the bridge. Remarkably, employing 16 pipe dampers, covering only 5% of the total beam length, results in a significant reduction up to 75% in the maximum deflection of the bridge, especially noticeable in systems with low initial flexural rigidity factors. The baseline in Figure 4 represents the maximum deflection at the mid-span of the initial beam without pipe dampers

(i.e., $K_n = 1$ and $n_{pipe} = 0$). The aim is to determine the flexural rigidity factor (K_n) at which the maximum deflection of the beam with pipe dampers matches with the baseline level. This reduction in K_n primarily arises from reducing the size of beam sections, assuming the slenderness of the base beam remains constant.

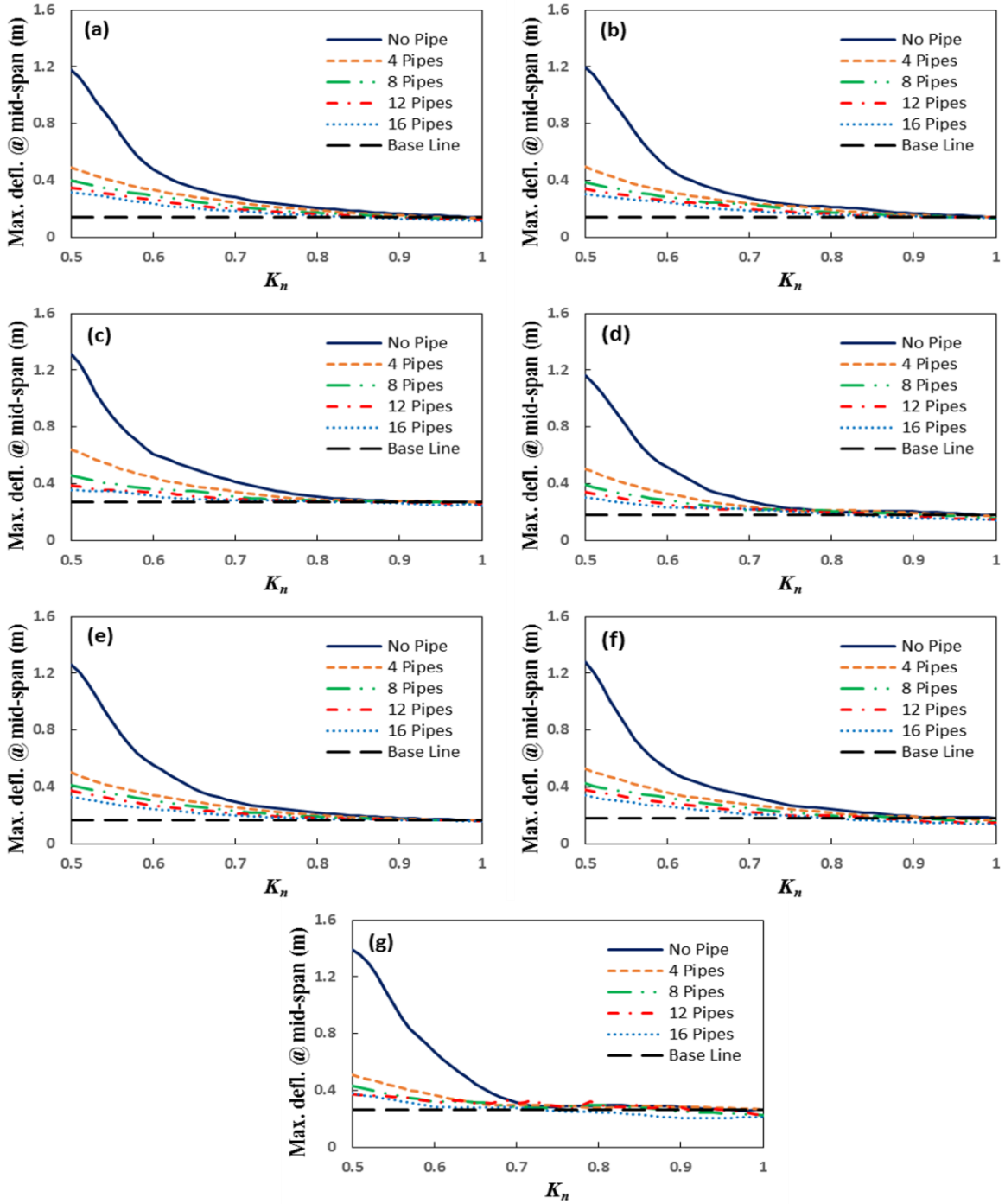

Fig. 4. Effect of Initial Flexural Rigidity Factor K_n on the variations of the beam deflection with and without steel pipe dampers a) L'Aquila, b) Imperial Valley, c) Kobe, d) Mammoth Lakes, e) Loma Prieta, f) Northridge, g) Tabas [5].

For easier comparison, Table 5 lists the necessary K_n Factor required for bridge systems equipped with 16 pipe dampers to achieve the same maximum mid-span deflection as the baseline over seven seismic records. It should be noted that the use of 16 pipe dampers allows for a reduction in the flexural rigidity of the main beams by up to 27%, with an average reduction of around 16%. According to Table 5, the efficiency of pipe dampers depends on

two main parameters: the factor of $V_s30\ (m/s)$ which is related to the type of construction soil, and the simultaneous effect (M_n), which has been fully investigated. In general, the efficiency of the SPDs increases with the influence of the vertical seismic excitation with the high value of M_n as well as in rocky soils associated with high $V_s30\ (m/s)$ factor.

Table 5. Effects of using Steel Pipe Dampers and Different Initial Flexural Rigidity K_n on the Maximum Bridge Deflection under Seven Selected Earthquakes [5].

Number	Event	V_s30 (m/s)	M_n (%)	K_n	n_{pipe}	Maximum mid-span deflection (m)
1	L'Aquila, Italy	488	3.8	1	0	0.138
				0.86	16	
2	Imperial Valley	213	6.0	1	0	0.141
				0.95	16	
3	Kobe, Japan	312	103	1	0	0.270
				0.83	16	
4	Mammoth Lakes	382	33.1	1	0	0.177
				0.83	16	
5	Loma Prieta	462	24.1	1	0	0.165
				0.9	16	
6	Northridge	298	35.3	1	0	0.180
				0.8	16	
7	Tabas, Iran	766	98.5	1	0	0.264
				0.73	16	

4. Conclusion

This study underscores the pivotal role of vertical earthquake components in the structural behaviour of bridges. Through numerical modelling, we observed a significant increase in maximum deflections under seismic excitation during bridge operation, as indicated by the M_n factor. Across seven near-field earthquake scenarios, simultaneous effects ranged from a 3.8% to a 103% increase, with notable peaks in Kobe and Tabas, reaching up to a 103% and a 98.5% increase, respectively. On the other hand, the average increase of simultaneous effects under all seven earthquakes shows a 73.6% rise in the realistic ratios of moving masses velocity and their masses ([0.05-0.35]), alongside a maximum value showcasing a 513.8% increase in this zone during the Tabas earthquake.

Additionally, statistical analysis was conducted to discern the variability of earthquake effects on bridge structures. Utilizing data from 100 selected earthquakes, regression analysis identified PGA_V and Earthquake Magnitude (M_w) as prominent influencers. This analysis facilitated the development of a linear regression model (Equation 6) for predicting structural responses under seismic conditions.

Furthermore, a novel vibration suppression method using steel pipe dampers (SPDs) was introduced, showcasing significant reductions in maximum deflections. Employing 16 pipe dampers at the mid-span of main beams resulted in noteworthy section reductions, underscoring their efficacy in mitigating vibrations. The efficiency of SPDs varied based on soil type ($V_s30\ (m/s)$) and simultaneous effects (M_n), with notable enhancements observed in regions with high $V_s30\ (m/s)$ and M_n values. In summary, our findings offer valuable insights for reassessing and designing bridge structures under dynamic loading conditions for structural health monitoring (SHM).

References

[1] Nikkhoo A, Farazandeh A and Ebrahimzadeh Hassanabadi M (2014), "On the computation of moving mass/beam interaction utilizing a semi-analytical method," J. Braz. Soc. Mech. Sci. Eng., 38(3): 761-771.

[2] Ichikawa M, Miyakawa Y and Matsuda A (2000), "Vibration analysis of the continuous beam subjected to a moving mass," J. Sound Vib., 230(3): 493-506.
[3] Zarfam R, Khaloo AR and Nikkhoo A (2013), "On the response spectrum of Euler-Bernoulli beams with a moving mass and horizontal support excitation" Mech. Res. Commun., 47: 77-83.
[4] Küttenbaum S, Braml T, Taffe A, Keßler S, Maack S. Reliability assessment of existing structures using results of nondestructive testing. Structural Concrete. 2021; 1–21.
[5] Nikkhoo A, Eskandari A.B, Farazandeh A, Hajirasouliha I (2019), "Vibration control of bridges under simultaneous effects of earthquake and moving loads using steel pipe dampers" Journal of Vibration and Control, 25:2580-2594.
[6] Legeron F and Sheikh MN (2009), "Bridge support elastic reactions under vertical earthquake ground motion," Eng. Struct., 31(10): 2317-2326.
[7] Stefan Küttenbaum, Stefan Maack, and Alexander Taffe (2022), "Approach to the development of a model to quantify the quality of tendon localization in concrete using ultrasound" MATEC Web of Conferences 364, 03007 ICCRRR 2022.
[8] Nikkhoo A, Rofooei FR and Shadnam M (2007), "Dynamic behavior and modal control of beams under moving mass," J. Sound Vib., 306(3): 712-724.
[9] Maleki S and Bagheri S (2010), "Pipe damper, Part I: Experimental and analytical study," J. Constr. Steel Res., 66(8): 1088-1095.